JOURNAL OF SOLID STATE CHEMISTRY 37, 77–84 (1981)

A Thermochemical Study of the Phase Reaction $TbO_{1.5+x}$ + (3/28 − x/2) O_2 → (1/7)Tb_7O_{12}

HIDEAKI INABA,* ALEXANDRA NAVROTSKY, AND LEROY EYRING

Department of Chemistry and Center for Solid State Science, Arizona State University, Tempe, Arizona 85281

Received December 20, 1979; in revised form June 9, 1980

The heat of reaction and equilibrium pressure for the oxidation reaction $TbO_{1.5+x}$ + (3/28 − x/2) O_2 → (1/7)Tb_7O_{12} have been measured by means of a Tian–Calvet-type calorimeter and a thermal balance. The results of the weight measurement show a reproducible hysteresis loop. The heat of reaction has been measured along the oxidation branch of the hysteresis loop. The partial molar enthalpy indicates four distinct compositional regions. First, the $TbO_{1.5+x}$ region which can be described in terms of a point defect model and strong interaction between neighboring excess oxygen atoms. Second, the region between $TbO_{1.54}$ and $TbO_{1.61}$ is interpreted as the intrinsic hysteresis region and discussed in terms of the regular solution model. Third, the region between $TbO_{1.61}$ and $TbO_{1.70}$ is recognized as a pseudophase region. Fourth, a region of ι phase exists in which the partial thermodynamic quantities can be compared with those of $CeO_{1.714}$, $PrO_{1.714}$, and $TbO_{1.714}$. The partial molar enthalpy was also measured for a scanning loop which is also interpreted in terms of the four regimes.

1. Introduction

The Tb–O system at oxygen pressures below one atmosphere has three phases as shown in Fig. 1, $TbO_{1.5+x}$ (Φ), $TbO_{1.714}$ (ι), and $TbO_{1.818}$ (δ), as well as marked stability at $TbO_{1.809}$ (δ'). The first three phases belong to a fluorite-related homologous series (*5*).

Thermodynamic studies of cyclic transformations between any two of these phases have shown that reproducible hysteresis loops are followed (*1–5*). Chemical hysteresis is far from being well understood in spite of its frequent occurrence in phase transformations. In order to understand the nature and mechanism of this phenomenon it is necessary to have a detailed knowledge of the structural, thermodynamic and kinetic relationships of the end members of the phase reaction. To this end, studies of the relationship between thermodynamics and kinetics have been pursued (*7, 8*).

The direct observation of the heat of reaction at known pressures (compositions) provides the most important thermodynamic properties $\Delta\bar{H}_{O_2}$, $\Delta\bar{G}_{O_2}$, and $\Delta\bar{S}_{O_2}$, respectively the partial molar enthalpy, Gibbs free energy, and entropy of oxygen in the oxide. The direct calorimetric enthalpies are more reliable than those derived from tensimetric measurements. Calorimetric studies have been done previously in systems such as ZrO_x (*10*), MnO_{1+x} (*11*), CeO_{2-x} (*12*), and UO_{2+x} (*13*). In the previous paper (*9*), these quantities for the ι–α

* On leave from the Department of Nuclear Engineering, Faculty of Engineering, Nagoya University, Furo-Cho Chikusa-ku Nagoya 464, Japan.

0022-4596/81/040077-08$02.00/0

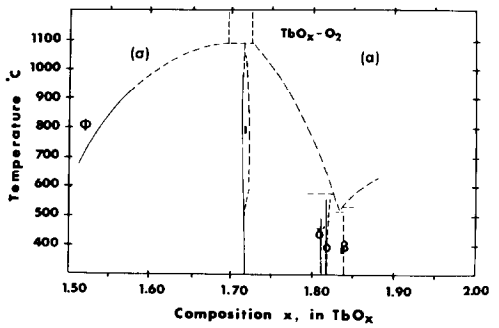

FIG. 1. Phase diagram of terbium oxide (see Ref. *1*, p. 623).

phase region of the praseodymium oxides were measured by means of a Tian–Calvet-type calorimeter and the nature of hysteresis was discussed in terms of the regular solution model (*14*). Oxygen partial pressure measurements as a function of temperature together with compositional measurements have also provided values for $\Delta\bar{H}_{O_2}$, $\Delta\bar{G}_{O_2}$, and $\Delta\bar{S}_{O_2}$, in systems such as PuO_{2-x} (*15*), NbO_{1+x} (*16*), AmO_{2-x} (*17*), and CeO_{2-x} (*18*). In the present study, the direct heat of reaction along the oxidation branch of the hysteresis loop, as well as an inner scanning loop, has been observed and the derived thermodynamic properties have been discussed.

2. Experimental

2.1 Calorimeter

The isothermal twin microcalorimeter of the Tian–Calvet type used in these experiments has been described elsewhere (*19, 20*). Some modifications of the specimen chamber were made to allow study of a solid–gas reaction. The quartz reaction tubes 19 mm i.d. and 86 cm long, are connected to a vacuum system through stopcocks and capillary tubes. The sample container is made of 22 platinum dishes 18.8 mm in diameter and 6 mm deep stacked with a platinum support. Oxygen gas is accessible to the oxide through 0.03-mm spaces between the dishes. The calorimetric sample is 22.3840 g of terbium oxide in the form of $TbO_{1.714}$. A correction for the heat effect associated with the addition of gas is eliminated by introducing the gas simultaneously into both the sample and reference side (*9*). The calorimeter is calibrated by dropping a piece of platinum into the sample chamber using the same-size quartz tube. The enthalpy change for platinum between 713°C and room temperature is calculated using standard reference data thus providing a calibration factor. The pressure was read by means of a Datametrics electronic manometer, the analogue signal of which was accurately digitized using a digital voltmeter.

The change of the O/Tb ratio was determined by an accurate pressure measurement and the predetermined dead volume of the reaction tube. The precision of the measurement of the O/Tb change due to reaction was estimated to be 2–5% depending on the change.

The 99.9% pure oxygen was supplied by the Liquid Air Co. and used without further purification. The terbium oxide was furnished by the Research Chemical Division of Nucor Co. as 99.999% pure with respect to other rare earths. Typical impurities of other elements are Fe, ND; Mg, Al, Ca, Si < 0.005. This oxide was precipitated as oxalate and reoxidized to obtain a dense powder, as described previously (*9*).

2.2 The Thermogravimetric Study

Thermodynamic measurement of terbium oxides (between the Φ and ι phases) was also carried out using a Cahn 1000 thermal balance, as described elsewhere (*7*). The same oxygen and oxide samples were used as in the calorimetric study. The sample consisted of 1.0554 g in the form of $TbO_{1.714}$.

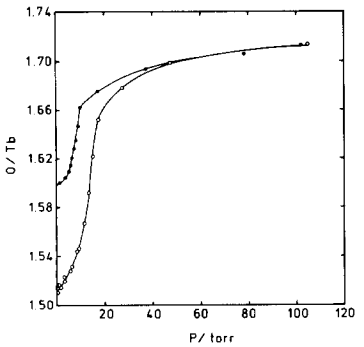

FIG. 2. Oxidation branches of the hysteresis and inner scanning loop between Φ and ι phases measured in the calorimeter at 713°C. ○, Complete loop; ●, scanning loop.

3. Results

3.1 The Isothermal Hysteresis Loop between the Φ and ι Phases

The composition of terbium oxide was measured as a function of oxygen pressure at 713°C by two different methods. One, obtained thermogravimetrically, is shown in Fig. 2, where the complete hysteresis loop of both oxidation and reduction paths is seen. The other, shown in Fig. 3, was determined by measuring the pressure change when oxygen gas was absorbed in or released from the solid in the calorimeter. Because of the slowness of the reaction, the reduction branch of the hysteresis loop was not measured in the calorimeter. Instead, the inner scanning loop (oxidation) was observed between $TbO_{1.6}$ and $TbO_{1.718}$, where the starting composition $TbO_{1.6}$ was obtained by the incomplete reduction from the ι phase. In neither case was the composition determined absolutely, but was assumed to be $TbO_{1.714}$ around 100 Torr, based on previous experience. As seen in Figs. 2 and 3, the agreement of the oxidation branch of the hysteresis loop between the two different methods is satisfactory.

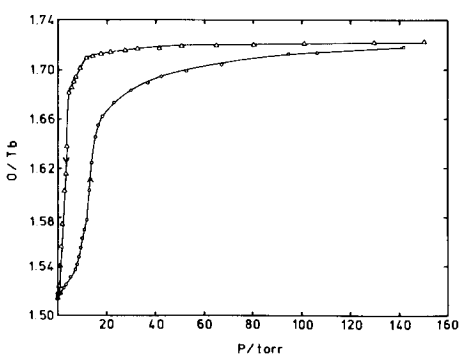

FIG. 3. Isothermal hysteresis loop measured by a thermal balance at 713°C. ○, Oxidation; △, reduction.

3.2 The Partial Thermodynamic Properties between the Φ and ι Phases

Examples of the calorimetric measurements are given in Table I. After the system has reached equilibrium the oxygen pressure is increased suddenly to both sides of the reaction tube, and the compositional change and heat generated are measured. Owing to the slowness of the reduction, it was difficult to detect the endpoint of the reaction. Specifically, the drift rate of the baseline was the same order of magnitude as the heat effect toward the end of the reaction. It was, therefore, not possible to obtain accurate data along the reduction path except for one point around $TbO_{1.7}$. One of the practical reasons the reduction was so slow under these conditions is that the volume of the calorimeter is limited and the pressure buildup as the reduction proceeds reduces the rate of an already very slow reaction. According to Boureau and Kleppa (*21*), the partial molar enthalpy should equal $Q/\Delta n$ taking into account the work done by the gas. Here Q is the heat absorbed and Δn the number of moles of O_2 absorbed by the solid instead of $((Q/\Delta n) - RT)$ which has been used so far. The partial molar enthalpy for the complete loop and an inner scanning loop is shown in Fig. 4. The reaction was relatively fast in the one-phase region and a stable baseline was obtained within 90 min after the initiation of the reaction. In

TABLE I

SOME EXAMPLES OF THE CALORIMETRIC RESULTS

Experiment number	Initial pressure (Torr)	Final pressure (Torr)	Compositional change ($\times 10^{-3}$)	Average composition x in TbO_x	Absorbed heat (cal)	Partial molar enthalpy (kcal/mole of O_2)
CO-1	0.117	0.830	2.7195	1.5155	−3.214	−19.68
CO-2	0.830	2.881	7.6854	1.5207	−9.101	−19.72
CO-3	2.881	6.494	7.6700	1.5284	−11.287	−24.50
CO-4	6.494	9.253	14.272	1.5394	−29.67	−34.64
CO-5	9.253	11.511	20.323	1.5567	−46.04	−37.72
CO-6	11.511	13.802	25.593	1.5796	−55.91	−36.37

the two-phase region more than 2 hr was required to obtain a stable baseline.

As seen in Fig. 4, the curve showing $-\Delta\bar{H}_{O_2}$ versus O/Tb can be divided into four regions: a region of sharp increase between $TbO_{1.51}$ and $TbO_{1.54}$, a region of gradual increase between $TbO_{1.54}$ and $TbO_{1.61}$, a region of intermediate increase between $TbO_{1.61}$ and $TbO_{1.70}$, and a flat region between $TbO_{1.70}$ and $TbO_{1.73}$. This tendency is in qualitative agreement with a previous work (*2*), where $-\Delta\bar{H}_{O_2}$ was obtained from the oxygen pressure measurement as a function of temperature at known compositions, except for the region where O/Tb is greater than 1.70. The partial molar free energy $\Delta\bar{G}_{O_2}$ is obtained from the isothermal hysteresis curve shown in Fig. 2 using the relationship $\Delta\bar{G}_{O_2} = RT \ln P_{O_2}$.

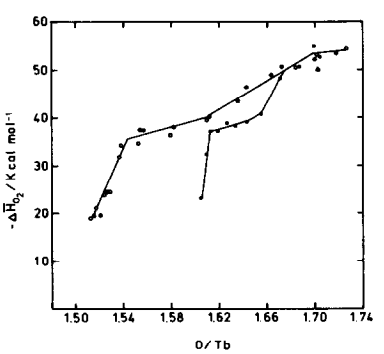

FIG. 4. Partial molar enthalpy as a function of composition. ○, Complete loop (oxidation); ●, scanning loop, △, complete loop (reduction).

From $\Delta\bar{G}_{O_2}$ and $\Delta\bar{H}_{O_2}$, the partial molar entropy $\Delta\bar{S}_{O_2}$ can be calculated, using the relationship

$$\Delta\bar{S}_{O_2} = \frac{\Delta\bar{H}_{O_2} - \Delta\bar{G}_{O_2}}{T}$$

4. Discussion

4.1 The Point Defect Model for the $TbO_{1.5+x}$ Region

As discussed in the previous paper (*9*), the point defect model should not be applied to compounds such as the rare earth oxides, R_nO_{2n-2} (n = 7–12) having extended defects. However, for hyperstoichiometric Φ phase of composition $TbO_{1.5+x}$, it might be possible to use the point defect model; namely one may assume that excess oxygen atoms randomly occupy the Z site (*22*) of the C-type (bixbyite) structure without any ordering. Endo *et al.* (*23*) interpreted the thermodynamic data of $Pr_{1-y}Gd_yO_{1.5+x}$ by assuming that the equilibrium between σ-phase oxide and oxygen can be expressed by

$$2\,Pr^{4+} + O_z^{2-} = 2\,Pr^{3+} + V_z + \tfrac{1}{2}\,O_2, \quad (1)$$

where O_z^{2-} denotes an oxygen ion occupying the Z site and V_z symbolizes the vacancy. They obtained essentially the partial molar enthalpy, $\Delta\bar{H}_{O_2}$, as a function of x in $Pr_{1-y}Gd_yO_{1.5+x}$ through the equilibrium

constant of Eq. (1). A plot of $\Delta\bar{H}_{O_2}$ against x follows a parabolic curve. According to their discussion, the enthalpy change $H(x)$ is expressed by

$$H(x) = -2N(\epsilon x + n\omega x^2), \qquad (2)$$

where N is Avogadros number, ϵ the energy required for introducing an atomic oxygen into the Z site to form an O_z^{2-} ion and two Pr^{4+} ions converted from Pr^{3+} ions, n the number of neighboring sites of an O_z^{2-} ion, and ω the interaction energy of two adjacent O_z^{2-} ions. When ϵ and ω are constant, the partial molar enthalpy dH/dx would give a straight line against x as can be seen from Eq. (2). In order to get a parabolic curve for dH/dx vs x, they assumed that ϵ and ω change with the volume of the crystal.

In the case of $Pr_{0.8}Gd_{0.2}O_{1.5+x}$, the phase of C-type structure extends up to $x = 0.18$ because the ordering of the oxygen atoms is prevented by the inclusion of Gd atoms. However, in the present case the upper limit of the Φ phase would be around $x = 0.04$, as seen from Figs. 2, 3, 4, and 5. When x is a smaller value; ϵ and ω would be constant as shown by the plot of dH/dx vs x for $Pr_{0.8}Gd_{0.2}O_{1.5+x}$ (*23*) which was almost a straight line below $x = 0.07$.

This treatment can be applied in the same way to the Tb–O system for O/Tb < 1.543 as shown in Fig. 4, where $-\Delta\bar{H}_{O_2}$ varies linearly with composition up to O/Tb = 1.543. One can expect that the interaction between excess oxygen atoms in $TbO_{1.5+x}$ is very strong, as indicated in Fig. 4 where $-\Delta\bar{H}_{O_2}$ at O/Tb = 1.543 is almost twice that at O/Tb = 1.513.

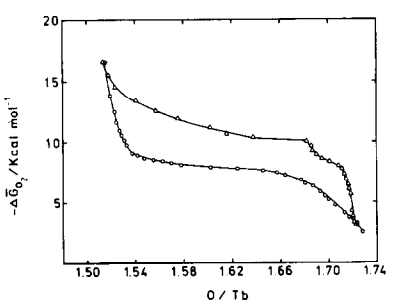

FIG. 5. Partial molar free energy as a function of composition. O, Oxidation; Δ, reduction.

4.2 Regular Solution Model in the Region $TbO_{1.54}$–$TbO_{1.61}$

The point defect model is no longer applicable beyond $TbO_{1.54}$, where the hyperstoichiometric Φ and ordered ι phases are believed to coexist (see Figs. 2, 3, and 4). In this region, the regular solution model may be applied as it has been previously (*9*, *14*).

This model can be applied to a mixture of A and B phases having appreciable interaction. When the reaction is represented in the following form:

$$MO_a + \tfrac{1}{2}bO_2 = MO_{a+b}, \qquad (3)$$

with $MO_a = A$ and $MO_{a+b} = B$, the Gibbs free energy of the system can be represented as

$$G = N_{O_2}\mu_{O_2} + N_A\mu_A + N_B\mu_B + \frac{N_AN_B}{N}\Gamma + (NkT/m)\{x_B \ln x_B + (1 - x_B)\ln(1 - x_B)\}, \qquad (4)$$

where N_A and N_B are the number of A and B, respectively, $N = N_A + N_B$, N_{O_2} is the number of moles of oxygen gas, μ_A and μ_B are the chemical potentials of A and B, respectively, $X_B = N_B/N$, Γ is the net interaction energy between A and B, and m is the minimum domain size, which behaves as m units of MO_a or MO_{a+b}. G is minimized by holding the total metal atoms, N, and the oxygen atoms $[2NO_2 + AN_A + (a + b)N_B]$, constant. The result is

$$\frac{b}{2}\mu_{O_2} = \frac{b}{2}kT \ln P_{O_2} = \mu_B - \mu_A + \Gamma(1 - 2x_B) + \frac{kT}{m}\ln\frac{x_B}{1 - x_B}. \qquad (5)$$

This gives three roots, if the proper values for $\mu_B - \mu_A$ and Γ are chosen.

Taking stable and metastable solutions (ignoring one unstable root), a hysteresis curve is obtained. In order to interpret the partial molar enthalpy data, the relation $\mu_A = \bar{H}_A - T\bar{S}_A$, etc. is substituted in Eq. (4), which can be rewritten as

$$G = \bar{H}_{O_2}N_{O_2}\bar{H}_AN_A + \bar{H}_BN_B\frac{N_AN_B}{N}\Gamma + \frac{NkT}{m}\{X_B \ln X_B + (1 - X_B)\ln(1 - X_B)\} - T\bar{S}_{O_2}N_{O_2} - T\bar{S}_AN_A - T\bar{S}_BN_B. \quad (6)$$

Dividing by N and abstracting the enthalpy part (H) of Eq. (6), we get

$$H = H_A(1 - X_B) + \bar{H}_BX_B + X_B(1 - X_B)\Gamma + \frac{N_{O_2}}{N}\bar{H}_{O_2}, \quad (7)$$

where $\bar{H}_{O_2}$ is the partial molar enthalpy of oxygen gas and

$$\bar{H}_{O_2} = \frac{\partial(\mu_{O_2}/T)}{\partial(1/T)} = k\frac{\partial \ln P_{O_2}}{\partial(1/T)}. \quad (8)$$

Taking the derivative of Eq. (7) in order to get the partial molar quantity, we have

$$\frac{b}{2}\Delta\bar{H}_{O_2} = \frac{dH}{dX_B} = -\bar{H}_A + \bar{H}_B + (1 - 2X_B)\Gamma - \frac{1}{2}bk\frac{\partial(\ln P_{O_2})}{\partial(1/T)} + \frac{N_{O_2}}{N}\frac{\partial^2(\ln P_{O_2})}{\partial(1/T)\,\partial X_B}, \quad (9)$$

where Γ is asumed to be independent of X_B. Equation (9) suggests that if the last two terms are sufficiently small, as in the case of PrO_x (*9*), and the interaction term Γ is negligibly small, the partial molar enthalpy would be constant in the two-phase region regardless of composition as is the case for α–Zr + ZrO_{2-y} (*10*), NbO + NbO_2, and NbO_2 + $NbO_{2.42}$ (*16*). However, as seen in Fig. 4, Γ is not negligibly small in this case and a gradual increase in $-\Delta\bar{H}_{O_2}$ is observed between $TbO_{1.54}$ and $TbO_{1.61}$ as in the Pr–O system (*9*). The slope of the $-\Delta\bar{H}_{O_2}$ vs O/Tb line depends on the magnitude of Γ, which in turn would depend upon the domain size and coherency of the boundary between the two phases.

4.3 Pseudophase Behavior Between $TbO_{1.61}$ and $TbO_{1.7}$

In previous studies (*3, 4*) pseudophase behavior has been observed between the Φ and ι phases of terbium oxide. (This designation is given to the almost linear region adjacent to a single-phase region in the temperature–composition diagram at isobaric conditions. A reproducible bivariant behavior is observed.) A high-temperature X-ray study (*3*) at 900°C on the oxidation path showed that the reaction $\Phi \rightarrow \iota$ was in progress at a pressure of 200 Torr ($\sim TbO_{1.60}$), but at 300 Torr ($\sim TbO_{1.67}$) if Φ were present the amount was too small to be detected (ι phase is more dominant than would be expected). Pseudophase behavior in this and closely related systems has been observed especially in oxidation and has been discussed in terms of coherently intergrown closely related structures (*1, 4*). In this view, during the final stages of reaction, the phase which is appearing isolates cores of the disappearing phase and pseudophase behavior results. This occurs in both directions, but it is much more pronounced when a phase with a larger molar volume is enclosed or when the crystal symmetry is lowered. It would be desirable to obtain detailed information about the structure of the pseudophase by using high-resolution electron microscopy. At the present time, however, one could postulate that in a pseudophase region the intergrowth between the two phases is markedly developed and coherency between the two phases is strengthened compared to that in the intrinsic two-phase region. If the regular solution model were applied to the pseudophase region, a larger interaction term, Γ (Eq. (8)), would be obtained. As can be seen in Fig. 4, the $-\Delta\bar{H}_{O_2}$ vs O/Tb

plot shows that there is a break in the curve around $TbO_{1.61}$ and the slope of the line between $TbO_{1.61}$ and $TbO_{1.7}$ is larger than that between $TbO_{1.54}$ and $TbO_{1.61}$, consistent with the above discussion.

4.4 Partial Molar Quantities of ι Phase

From Figs. 4, 5, and 6, we obtain the $-\Delta\bar{G}_{O_2}$, $-\Delta\bar{H}_{O_2}$, and $-\Delta\bar{S}_{O_2}$ of $TbO_{1.714}$. The results are listed in Table II, where the corresponding data for $CeO_{1.714}$ (*12, 25*) and $PrO_{1.714}$ (*9*) are also given for comparison. The data for $CeO_{1.714}$ cannot be immediately compared with others because of the difference in the reaction temperature, however, this value is suitable for a qualitative discussion. Since $-\Delta\bar{G}_{O_2}$ indicates the degree of the stability of the oxides, $CeO_{1.714}$ is much more stable than the others and $PrO_{1.714}$ is slightly more stable than $TbO_{1.714}$. Among rare earths only these three oxides display the ι phase. The value of $-\Delta\bar{G}_{O_2}$ of the ι phase would depend on the stability of R^{4+}, the extent of removal of $4f$ electrons. The great stability of $CeO_{1.714}$ shows that Ce^{4+} ($4f^0$) is very stable. $-\Delta\bar{S}_{O_2}$ indicates the degree of order of the oxygen sublattice and it should be constant among these three oxides since they are isostructural (*6, 26*). However, there is considerable difference between $PrO_{1.714}$ and $TbO_{1.714}$ which must be assigned to vibrational contributions.

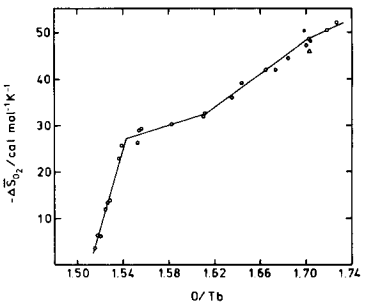

FIG. 6. Partial molar entropy as a function of composition. ○, Complete loop (oxidation); △, complete loop (reduction); ●, scanning loop.

4.5 An Inner Scanning Loop

The intrinsic hysteretic behavior of the rare earth oxide results in scanning (*2, 4, 5*) loops when reversal occurs before the cycle is completed. An oxidation branch of a scanning loop was observed between $TbO_{1.6}$ and $TbO_{1.714}$, as shown in Fig. 2, where the reaction was reversed before the single phase, Φ, was reached. The shape of the loop is similar to that of the completed loop, but the inflection points are shifted to slightly lower pressures. Similar phenomena are often seen in isobaric curves (*4*).

The scanning loop may be interpreted as follows. At the original point ($TbO_{1.60}$) the system includes some fraction of the Φ phase ($TbO_{1.5+x}$) as well as the ι phase (Tb_7O_{12}) because of the low "equilibrium

TABLE II

PARTIAL THERMODYNAMIC QUANTITIES OF ι PHASE OF RARE EARTH OXIDES

	$-\Delta\bar{G}_{O_2}(O_2)$ kcal mole^{-1}	$-\Delta\bar{H}_{O_2}(O_2)$ kcal mole^{-1}	$-\Delta\bar{S}_{O_2}(O_2)$ cal K^{-1} mole^{-1}	Reference
$CeO_{1.714}$ (at 1080°C)	114	164	37	(*12, 25*)
$PrO_{1.714}$ (at 713°C)	8	27	19	(*9*)
$TbO_{1.714}$ (at 713°C)	4	54	50	This work

pressure," although in the complete loop there is no pure Φ phase left at the same composition. When the pressure is increased to about 5 Torr ($\sim TbO_{1.61}$), the Φ phase has been oxidized to its upper composition limit. Between $TbO_{1.61}$ and $TbO_{1.66}$ the intergrown two-phase region exists. At about 10 Torr ($\sim TbO_{1.66}$) pseudophase behavior is observed and the scanning loop approaches slowly the intrinsic loop. The $-\Delta\bar{H}_{O_2}$ vs O/Tb curve for the scanning loop should reflect this behavior.

At lower oxygen content ($TbO_{1.605} - TbO_{1.613}$), since the system includes some fraction of Φ phase, the values of $-\Delta\bar{H}_{O_2}$ should be similar to those of the Φ phase of the intrinsic loop. The fraction of the Φ phase is so small that the $-\Delta\bar{H}_{O_2}$ vs O/Tb curve has a steeper slope in this case. Between $TbO_{1.613}$ and $TbO_{1.656}$, the intergrowth of the Φ and ι phases yields the same characteristics in the $-\Delta\bar{H}_{O_2}$ vs O/Tb plot as in the intrinsic loop in the same phenominological region but it occurs over a smaller compositional range. At $TbO_{1.656}$ the pseudophase behavior starts and the values of $-\Delta\bar{H}_{O_2}$ approach those of the intrinsic loop rapidly as O/Tb increases.

Acknowledgment

This work was supported by the National Science Foundation through Grants DMR 78-05722 and DMR 78-10038.

References

1. B. G. Hyde and L. Eyring, *in* "Rare Earth Research, III" (L. Eyring, Ed.), p. 623, Gordon & Breach, New York, (1966).
2. J. Kordis and L. Eyring, *J. Phys. Chem.* **72**, 2044 (1968).
3. D. A. Burnham, L. Eyring, and J. Kordis, *J. Phys. Chem.* **72**, 4424 (1968).
4. A. T. Lowe and L. Eyring, *J. Solid State Chem.* **14**, 383 (1975).
5. A. T. Lowe, K. H. Lau, and Eyring, *J. Solid State Chem.* **15**, 9 (1975).
6. P. Kunzmann and L. Eyring, *J. Solid State Chem.* **14**, 229 (1975).
7. H. Inaba, S. P. Pack, S. H. Lin, and L. Eyring, *J. Solid State Chem.* **33**, 295 (1980).
8. H. Inaba, S. H. Lin, and L. Eyring, *J. Solid State Chem,* **37**, 58 (1981).
9. H. Inaba, A. Navrotsky, and L. Eyring, *J. Solid State Chem.* **37**, 67 (1981).
10. G. Boureau and P. Gerdanian, *High Temp. High Press* **2**, 681 (1970).
11. C. Picard and P. Gerdanian, *J. Solid State Chem.* **11**, 190 (1974).
12. J. Campserveux and P. Gerdanian, *J. Chem. Thermodyn.* **6**, 795 (1974).
13. P. Gerdanian and M. Dodé, "Thermodynamics of Nuclear Materials" p. 41, Intern. At. Energy Agency, Vienna (1968).
14. D. R. Knittel, S. P. Pack, S. H. Lin, and L. Eyring, *J. Chem. Phys.* **67**, 134 (1977).
15. M. H. Rand, Atomic Energy Review, Vol 4 Special Issue No. 1, Intern. At. Energy Agency, Vienna (1966).
16. J. F. Marucco, R. Tetot, P. Gerdanian, and C. Picard, *J. Solid State Chem.* **18**, 97 (1976).
17. T. D. Chikalla and L. Eyring, *J. Inorg. Nucl. Chem.* **29**, 2281 (1967).
18. D. J. M. Bevan and J. Kordis, *J. Inorg. Nucl. Chem.* **26**, 1509 (1964).
19. A. Navrotsky, *Earth Planet. Sci. Lett.* **19**, 471 (1973).
20. A. Navrotsky, *Phys. Chem. Minerals* **2**, 89 (1977).
21. G. Boureau and O. J. Kleppa, *J. Chem. Thermodyn.* **9**(6), 543 (1977).
22. K. Endo, S. Yamaucki, K. Fueki, and T. Mukaibo, *Bull. Chem. Soc. Japan* **49**(5), 1191 (1976).
23. K. Endo, S. Yamauchi, K. Fueki, and T. Mukaibo, *Bull. Chem. Soc. Japan 49* (9), 2379 (1976).
24. B. G. Hyde, D. J. M. Bevan, and L. Eyring, *Philos. Trans. Roy. Soc. London* **259**, 583 (1966).
25. J. Campserveux and P. Gerdanian, *J. Solid State Chem.* **23**, 73 (1978).
26. S. P. Ray and D. E. Cox, *J. Solid State Chem.* **15**, 333 (1975).